2026 IEEE International Conference on Robotics and Automation (ICRA 2026)
June 1-5, 2026. Vienna, Austria

Relaxation Dynamics in Oblate Spherical Rolling Robots

Micah J. Oevermann and Robert O. Ambrose

***Abstract*— Spherical robots rolling on flat ground often exhibit a wobbling motion that, at higher speeds, can escalate into end-over-end flipping. This paper proposes a fundamental dynamic cause of this instability: a relaxation effect analogous to the Intermediate Axis Theorem. Rotating bodies with oblate inertial profiles under dissipative loads tend to reorient toward spinning about their major moment of inertia, leading to the observed wobbling in spherical robots. While relaxation dynamics are well-studied in satellites and asteroids, this effect has not been previously applied to rolling systems. We extend these methods to constrained spherical robots, derive the governing dynamics, and conduct experiments with an empty shell on a slope and a reduced pendulum on flat ground and in water to aid in the discussion. Results suggest that translational rolling constraints act as a pseudo-dissipative load to drive the relaxation effect. This work bridges the fields of satellite dynamics theory and ground robotics, providing new insights into the stability of high-speed rolling robots to influence future hardware and control design choices.**

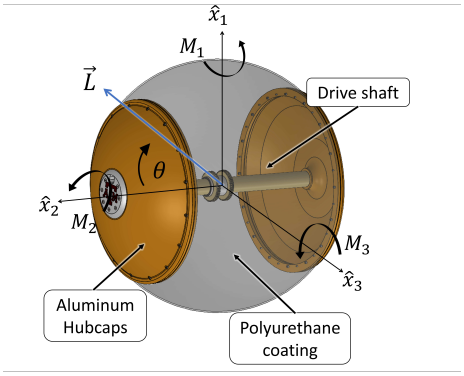

Fig. 1. Diagram of a robot shell's body frame with angular momentum vector L, applied moment components M_i, and relaxation angle θ, between the momentum and minimum inertia axis $\hat{x}_2$. The inertia about $\hat{x}_{1,3}$ are equal and greater than about $\hat{x}_2$.

I. Introduction

The bizarre rotational motion of free-flying tri-axial objects is a unique and well-studied phenomenon. Known as the Dzhanibekov effect, tennis racket, or the Intermediate Axis theorem, an object rotating about its intermediate moment of inertia will tend to flip from one side to the other [1]. Additionally, free-flying rotating objects under some form of dissipative load will eventually settle into rotation about their major moment of inertia to minimize kinetic energy. Cigar-shaped satellites, such as Explorer I, were initially set spinning about their minor moment of inertia; however, energy dissipated by structural vibrations in its antenna caused the satellite to attempt to settle into rotations about its major inertial axis. Study of this dissipative relaxation toward maximal-inertia rotation effect has had a lasting impact on spin-stabilized satellite design and Eulerian mechanics theory [2]. This is also recognized by astronomers studying spinning asteroids. In that field, the use of a "relaxation angle" or the angle of the angular momentum expressed in the body frame relative to an inertia axis is used to classify asteroid spin states and study their dynamics [3]. The techniques and intuition for studying complex rotations of free-flying objects could offer a refreshing perspective on the dynamic behavior of rolling robots.

Spherical robots have gained popularity over the past few years, see reference [4] for an excellent review. Generally, they are designed with an outer shell and an inner mechanism to generate rolling torque. Figure 1 shows an example schematic of a shell from a spherical robot called RoboBall that is driven by a pendulum; this shell is inflatable with a soft polyurethane coating as its primary rolling surface [5]. It would be reasonable to assume that a rotating object constrained to roll on a surface would display characteristics of the Intermediate Axis Theorem, especially if that object (or robot) is of non-uniform inertia. However, studies on spherical robots have either not addressed these effects directly or ignored them by assuming uniform inertia in their dynamic models. The next paragraphs will discuss several spherical robots and comment on whether they used a full 3D model or approximated a sphere as two cylinders for a decoupled approach. Since the inertia profile of a body is a driving factor behind the Dzhanibekov effect, the inertia tensors of the outer shells of their robots, as reported in their papers, will also be provided.

Arif et al. employed a flywheel with a decoupled model to reduce oscillations and achieve higher speeds [6]; however, they did not report the shell's inertial profile, instead focusing on the flywheel. Asiri developed a full dynamic model with a control scheme based on centripetal forces, but observed no unexpected motion in their experiments. Their robot had an almost uniform, slightly oblate profile [7]. Belzile used a fully coupled model and stated that the inertia was uniform, although photographs in their paper show a shaft across the sphere, which would alter the final inertia [8]. Feng also presented a full model, but simplified it enough to reduce it to an uncoupled system. While no inertia values were provided, their kinetic energy formulation (eq. 21 in [9]) implies unequal inertias.

B. Li adopted a Lagrangian formulation with kinematic

**Research supported by the Texas A&M Chancellor's Research Initiative and matching funds from the Texas Governor's University Research Initiative.

Authors are with Texas A&M University, College Station TX, US

constraints embedded directly into the derivation. They briefly acknowledged a wobbling behavior during turns but did not analyze it further, instead focusing on their novel jumping mechanism [10]. As a result, no internal inertial profiles were reported. Wang followed a decoupled approach, modeling the sphere as a cylinder and therefore reported only one inertia [11]. Ylikorpi introduced a soft-shell robot similar to the one shown in Figure 1, featuring an inflatable outer shell. Their model considered only one plane of motion but noted that the inertia could vary with inflation pressure and shell geometry [12].

Schroll constructed a full 3D model and observed what he coined as a "nutation instability" where the robot would excessively wobble at high speeds until it flipped hubcap to hubcap [13]. Singhal constructed a model similar to Schroll's, but arrived at the opposite conclusion that these effects would die out at higher speeds, although the claim was not supported by experiments with their prototype [14].

A summary of these studies is given in Table I. For those works that do provide inertial values, the axes have been redefined so that the middle inertia (I_2) is aligned with the robot's primary intended rolling direction, similar to Figure 1 along $\hat{x}_2$.

TABLE I
REPORTED INERTIAL PROFILES OF OUTER SHELLS

Ref. (year)	Model Type	Inertial Profile $[kg-m^2]$ $[I_1,\ I_2,\ I_3]$
[6] (2023)	Uncoupled	Not given
[11] (2023)	Uncoupled	[N/A, 0.888, N/A]
[9](2021)	Uncoupled	non-uniform via eq. 21
[12] (2017)	Uncoupled	$[\text{N/A}, (5.85-7.18)e^{-2}, \text{N/A}]$
[14] (2023)	Coupled	Uniform Inertia
[8] (2022)	Coupled	$[0.25, 0.25, 0.25]$
[7] (2019)	Coupled	$[2.65, 2.57, 2.65]e^{-2}$
[10] (2009)	Coupled	Not given
[13] (2009)	Coupled	$[0.25, 0.15, 0.25]$
	This Paper	$[1.04, 0.64, 1.04]$

From the list of inertial profiles in the table, it is clear that the possible inertial effects of the various robots' rotating outer shells have not been adequately studied or have been ignored entirely by using an uncoupled model. Developing a thorough understanding of the effect can influence the proper inertial profile necessary for rolling robots at higher speeds. The remainder of this paper will review useful dynamic analysis techniques used when studying the Intermediate Axis theorem. Then, it will extend those methods by applying rolling constraints and provide a discussion on the differences between the two cases. Additional experiments will be presented to explore the relationship between an inertially dissimilar object and its natural rolling stability.

II. DYNAMIC ANALYSIS OF ROTATING BODIES SUPPLEMENTED WITH RELAXATION DYNAMICS

This section juxtaposes two modeling paradigms: one derived from Euler's rotation equations and the other from relaxation dynamics, as presented by Likins in [2]. Both models will use the notation illustrated in Figure 1. Where the body frame axes are given by $\hat{x}_i$, and the net moments and angular velocities about the axes are given by M_i or ω_i for the i^{th} axis. Euler's equations use the individual components, while the relaxation dynamics will use the angle θ between the angular momentum vector. This vector is defined in equation (1), and similar statements can be made for the vectors of $\mathbf{M}$ and $\boldsymbol{\omega}$.

$$\mathbf{L} = I\boldsymbol{\omega} = I_1\omega_1\hat{x}_1 + I_2\omega_2\hat{x}_2 + I_3\omega_3\hat{x}_3 \tag{1}$$

A. Euler Dynamics of a Rotating Body Under Dissipation

The motion of a spinning body under the influence of external moments is described by Euler's equations, which are presented below. Here I is the inertia tensor of the rotating body.

$$I\dot{\boldsymbol{\omega}} + \boldsymbol{\omega} \times I\boldsymbol{\omega} = \mathbf{M} \tag{2}$$

However, from Table I most spherical robots are not inertially tri-axial; rather, they are ordered by $I_1 = I_3 > I_2$. Inertial profiles of this form are commonly referred to as "oblate" objects.

Consider a case where a satellite is under uniform structural damping, so that the effect can be modeled with (3). Here, C is a diagonal matrix of positive damping constants.

$$\mathbf{M} = -C\boldsymbol{\omega} \tag{3}$$

To examine the stability of free rotations with equation (2), assume constant rotation about ω_2 with small perturbations in ω_1 and ω_3 as δ_1 and δ_3 respectively. Ignoring $\delta_1\delta_3$ terms as negligible yields the dynamics in the form of $\dot{x} = A(\omega)x$, shown in (4).

$$\begin{pmatrix}\dot{\delta}_1\\ \dot{\omega}_2\\ \dot{\delta}_3\end{pmatrix} = I^{-1}\begin{bmatrix}-c & 0 & (I_2-I_3)\omega_2\\ 0 & -c & 0\\ (I_1-I_2)\omega_2 & 0 & -c\end{bmatrix}\begin{pmatrix}\delta_1\\ \omega_2\\ \delta_3\end{pmatrix} \tag{4}$$

So the eigenvalues of this system are given by

$$\zeta_1 = -c \tag{5a}$$

$$\zeta_{2,3} = -c \pm |\omega_2|\sqrt{(I_2-I_3)(I_1-I_2)} \tag{5b}$$

If the inertias are distinct and ordered ($I_3 > I_2 > I_1$), the radical will stay real so that one of the eigenvalues could become positive for large enough speeds of ω_2. This is the essence of the "flipping" observed in the Intermediate Axis Theorem.

However, if the inertias are oblate ($I_3 = I_1 > I_2$), then (5b). takes the form of (6). So that the troublesome radical term becomes imaginary. Yet, the real parts are still negative, so rotations about that axis are stable, albeit with some decaying harmonics.

$$\zeta_{2,3} = -c \pm i|\omega_2|\sqrt{(I_2-I_1)^2} \tag{6}$$

Thus, while free oblate bodies appear stable in the velocities, the relaxation dynamics shift the stability picture.

B. Relaxation Dynamics of a Damped Oblate Body

Defining a relaxation angle offers insight into the evolution of a body's rotational profile over time. In astrophysics, this angle is typically defined as the angle between the body's angular momentum vector and its greatest moment of inertia, see reference [3]. Most spherical robots roll about their minimum moment of inertia as shown in Table I. This section will redefine the relaxation angle with respect to that axis, rather than the maximum axis. The angle, angular momentum vector, and shell body frame are shown in Figure 1. When defined in this way, if the robot is rolling forward or driving straight, then $\mathbf{L}$ is aligned purely along $\hat{x}_2$, and the angle is zero. Likewise, if the shell is flipping end over end, then the vector would lie in the $\hat{x}_1 - \hat{x}_3$ plane, and the angle would be 90°. A schematic demonstrating these characteristics is shown in Figure 2.

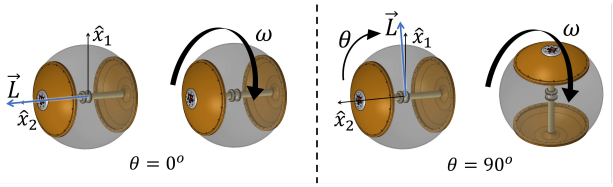

Fig. 2. A robot shell in two edge case relaxation states

The angle, θ, is calculated directly with (7).

$$\cos(\theta) = \frac{I_2\omega_2}{||L||} \tag{7}$$

Where $||L||$ is the norm of the angular momentum, given by (8).

$$||L||^2 = \boldsymbol{\omega}^T I^2 \boldsymbol{\omega} = I_1^2(\omega_1^2 + \omega_3^2) + I_2^2\omega_2^2 \tag{8}$$

With the rotational kinetic energy, T, given by (9).

$$2T = \boldsymbol{\omega}^T I \boldsymbol{\omega} = I_1(\omega_1^2 + \omega_3^2) + I_2\omega_2^2 \tag{9}$$

The relaxation angle θ can be expressed in terms of T and $||L||$ following an identical procedure shown by Likins in Section IV of [2]. The resulting relationship is expressed in (10) for our definition of the angle.

$$\cos^2(\theta) = \frac{I_2(2I_1T - ||L||^2)}{||L||^2(I_1 - I_2)} \tag{10}$$

If the change in momentum is small, then (10) can be differentiated directly to (11) as shown in Likins.

$$\dot{\theta} = \frac{2}{\sin(2\theta)} \frac{I_1 I_2}{||L||^2(I_2 - I_1)} \dot{T} \tag{11}$$

This equation is the *relaxation dynamics* of a rotating body. It is a tool to study the evolution of a rotating oblate body's rotational profile over time.

The behavior of equation (11) can be studied by separating it into three terms and determining their signs: the sinusoidal fraction, the inertia ratio, and the rate of change of angular kinetic energy. The first part, the sinusoid ratio, is positive within the quadrant between $\hat{x}_2$ and the $\hat{x}_1 - \hat{x}_3$ plane. For the inertia ratio, $||L||^2$ is always positive. Therefore, the sign of this term depends on the ordering of the inertias. For spherical robots, $I_1 > I_2$, so this term is negative. That leaves the stability of (11) down to the rate of rotational kinetic energy change, $\dot{T}$. This can be expressed in terms of the applied moment to the body using equations (2) and (9) and shown in (12).

$$\begin{aligned} 2\dot{T} &= \dot{\boldsymbol{\omega}}^T I \boldsymbol{\omega} + \boldsymbol{\omega}^T I \dot{\boldsymbol{\omega}} \\ \dot{T} &= \boldsymbol{\omega}^T I \dot{\boldsymbol{\omega}} \\ &= \boldsymbol{\omega}^T (M - \boldsymbol{\omega} \times (I\boldsymbol{\omega})) \\ \dot{T} &= \boldsymbol{\omega}^T M \end{aligned} \tag{12}$$

As with the eigenvalue analysis, apply uniform damping to the system to mimic the structural dissipation of a satellite, as shown in equation (3). So the relaxation dynamics become

$$\dot{\theta} = \frac{2}{\sin(2\theta)} \frac{I_1 I_2}{||L||^2(I_2 - I_1)} (-\boldsymbol{\omega}^T C \boldsymbol{\omega}) \tag{13}$$

The term $-\boldsymbol{\omega}^T C \boldsymbol{\omega}$ is negative definite for all non-zero $\boldsymbol{\omega}$. The positive sine term, negative inertia ratio, and negative dissipation terms net a positive sign for $\dot{\theta}$. Therefore, a rotating floating body under dissipation will experience a reduction in angular magnitude, but a shift in net rotational direction towards the $\hat{x}_1 - \hat{x}_2$ plane. As a robot's shell rotates under some dissipative load, it will shift to flip hubcap-to-hubcap, illustrated by Figure 2.

C. Comparing Responses of Rotation and Relaxation Dynamics

Figure 3 shows results from numerically integrating (2) with a uniform dissipation term, as defined by (3). The middle and right of the figure show the relaxation angle according to equation (7) and rotational kinetic energy defined by (9). The integrations use the inertia from Table I for this paper and chooses $c_i = 0.05$ for illustrative purposes.

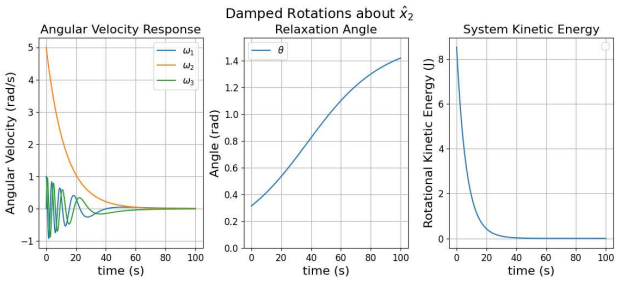

Fig. 3. Free body stable, but damped system drifts toward relaxation

The system is damped, so the velocities and the kinetic energy decay. However, as it slows, the relaxation angle increases, so the body transitions from rotating purely about the drive axis to flipping from hubcap-to-hubcap before coming to a stop.

III. Relaxation Dynamics for Rolling Oblate Bodies

The previous section introduced relaxation dynamics to study the behavior of free-flying objects under uniform damping. Since spherical robots are not satellites, the theory will need to be extended to the rolling case. This section will bridge that gap by applying appropriate constraints for a sphere rolling on a surface.

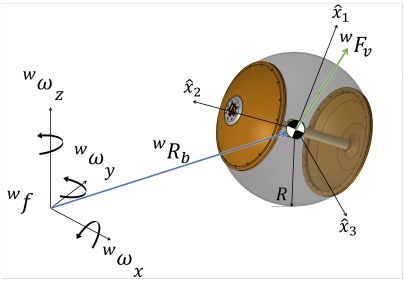

Fig. 4. The robot shell located in the world frame

A. Rolling Constraint and Contact Jacobian

Figure 4 illustrates the motion of a robot's shell within the world frame. For the remainder of this section, values expressed in the world or inertial frame will be preceded with a superscript ${}^w(\cdot)$. Values expressed in the body frame will have no superscript to remain consistent with the previous sections. When a sphere rolls without slipping on a plane, the translational velocity ${}^w\mathbf{v}$ is related to its rotational velocity in the world frame by equation (14), where R is the nominal outer shell radius.

$$ {}^w\mathbf{v} = \bar{R}\ {}^w\boldsymbol{\omega} \tag{14}$$

where

$$\bar{R} = \begin{bmatrix} 0 & R & 0 \\ -R & 0 & 0 \\ 0 & 0 & 0 \end{bmatrix},$$

Defining ${}^wR_b$ as a transform from the body frame to the world frame, express (14) in the form of (15) with respect to the body angular velocities.

$$ {}^w\mathbf{v} = \bar{R}\,{}^wR_b\,\boldsymbol{\omega} \tag{15}$$

Define the generalized velocity vector

$$\dot{q} = \begin{bmatrix} {}^w\mathbf{v} \\ \boldsymbol{\omega} \end{bmatrix} \tag{16}$$

The constraints can be written compactly as a contact Jacobian in (17), where eye_3 represents the identity matrix of size three. This notation is introduced to keep it distinct from the body inertia tensor I.

$$J(q)\dot{q} = 0, \qquad J(q)^T = \begin{bmatrix} \text{eye}_3 \\ -(\bar{R}\,{}^wR_b)^T \end{bmatrix} \tag{17}$$

B. Constrained Dynamics

The equations of motion with constraints then take the form

$$A(q)\ddot{q} + H(q,\dot{q}) = F + J^T\lambda, \tag{18}$$

with a block-diagonal mass matrix

$$A = \begin{bmatrix} m\ \text{eye}_3 & 0 \\ 0 & I \end{bmatrix}, \tag{19}$$

where m is the mass and I is the inertia tensor in the body frame of the robot's shell.

Splitting into linear and angular components in (20). Here m is the shell mass, ${}^wF_v$ are applied linear forces in the world frame, such as gravity, and λ are Lagrange multipliers representing constraint forces [15]. The other angular terms are consistent with equation (2).

$$m\,{}^w\dot{\mathbf{v}} = {}^wF_v + \lambda \tag{20a}$$

$$I\dot{\boldsymbol{\omega}} + \boldsymbol{\omega}\times(I\boldsymbol{\omega}) = M - (\bar{R}\,{}^wR_b)^T\lambda \tag{20b}$$

Combining equation (20), gives the reduced rotational dynamics:

$$I\dot{\boldsymbol{\omega}} + \boldsymbol{\omega}\times(I\boldsymbol{\omega}) = M - (\bar{R}\,{}^wR_b)^T(m\,{}^w\dot{\mathbf{v}} - {}^wF_v) \tag{21}$$

C. Expression for Angular Kinetic Energy Rate

Redefine the kinetic energy rate following a similar procedure from equation (12).

$$\dot{T} = \boldsymbol{\omega}^T M - \boldsymbol{\omega}^T(\bar{R}\,{}^wR_b)^T(m\,{}^w\dot{\mathbf{v}} - {}^wF_v) \tag{22}$$

Postmultiply the rolling constraint, eq. (15), with ${}^w\dot{\mathbf{v}}$ to obtain (23).

$${}^w\mathbf{v}^T\,{}^w\dot{\mathbf{v}} = \boldsymbol{\omega}^T(\bar{R}\,{}^wR_b)^T\,{}^w\dot{\mathbf{v}} \tag{23}$$

Translational kinetic energy is expressed as

$$T_{trans} = \frac{1}{2}m\,{}^w\mathbf{v}^T\,{}^w\mathbf{v} \tag{24}$$

The relationship between (23) and (24) can be shown directly below.

$$-\boldsymbol{\omega}^T(\bar{R}\,{}^wR_b)^T m\,{}^w\dot{\mathbf{v}} = -m\,{}^w\mathbf{v}^T\,{}^w\dot{\mathbf{v}} = -\frac{d}{dt}\left(\frac{1}{2}m\,{}^w\mathbf{v}^T\,{}^w\mathbf{v}\right)$$

That reduces down to the rate of change in kinetic energy.

$$-\boldsymbol{\omega}^T(\bar{R}\,{}^wR_b)^T m\,{}^w\dot{\mathbf{v}} = -\dot{T}_{trans} \tag{25}$$

Using the connection from (25), equation (22) can be written more descriptively as (26).

$$\dot{T} = \boldsymbol{\omega}^T M - \dot{T}_{trans} + \boldsymbol{\omega}^T(\bar{R}\,{}^wR_b)^T\,{}^wF_v \tag{26}$$

This highlights the additional effects rolling introduces on the system's angular kinetic energy. The angular power from the body frame moments remains the same as before, but now includes the energy siphoned to translational rolling motion (which behaves like an additional dissipative term), as well as the work done by linear forces mapped into the system. The relaxation stability of a rolling object is still dependent on a positive sign of $\dot{T}$.

D. Interpreting Linear Forces

If the system is rolling unpowered down a slope and the global coordinate frame and initial body frame are aligned along the angle of the slope, as shown in Figure 5. Then ${}^{w}R_b = eye_3$ and the only other force doing work on the system through ${}^{w}F_v$ is gravity, shown in (27) with α as the constant incline angle.

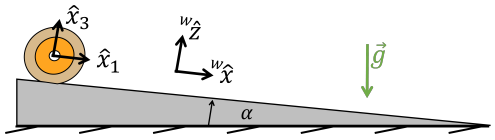

Fig. 5. World frame aligned with object rolling down slope

$$ {}^{w}F_v = \begin{pmatrix} mg\sin(\alpha) \\ 0 \\ -mg\cos(\alpha) \end{pmatrix} \tag{27} $$

the final term in (26) can be simplified to

$$ \boldsymbol{\omega}^T(\bar{R}\,{}^{w}R_b)^T{}^{w}F_v = \omega_2 mgR\sin(\alpha) \tag{28} $$

To study the stability of a rolling object, in this case, the sign of (29) must be positive. Assuming that the soft contact between the polyethylene shell and the concrete can be modeled close enough with the dissipative effect in (3).

$$ \dot{T} = -\boldsymbol{\omega}^T C\boldsymbol{\omega} - \dot{T}_{trans} + \omega_2 mgR\sin(\alpha) \tag{29} $$

From equation (29), all variables in the final gravity term are positive and will stay positive as ω_2 increases down the slope. However, as the object accelerates down the ramp, $\dot{T}_{trans}$ will also be positive along with the quadratic damping term. At fast enough speeds, $\dot{T}_{trans}$ and the quadratic damping term will overpower the linear-in-velocity gravity term, resulting in a negative sign for $\dot{T}$. In this case, the system will experience the relaxation effect and flip hubcap-to-hubcap.

This is counterintuitive to the free-flying object scenario. If the relaxation dynamics from (11) are considered without accounting for the translational coupling between the angular and translational components, intuition would assume that the net angular kinetic energy would increase as the system rolls down the slope, stabilizing the system. The next section supports the significance of including the translational term in equation (29) by an experiment with the robot shell.

IV. Shell Rolling Experiments

To verify (29), a series of experiments was conducted with only the robot's shell. A VN-100 IMU was mounted inside the robot's hubcaps to directly measure $\boldsymbol{\omega}$ with its onboard gyroscopes. The additional weight was balanced to keep the inertial profile as close to oblate as possible, but only accounted for an additional $0.62kg$ on the total system mass of $17.16kg$. A schematic of this setup is shown in Figure 6. A bare shaft was used in place of a drive mechanism to keep the shell's shape and nominal outer radius of $0.31m$.

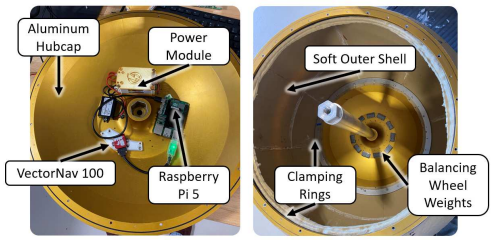

Fig. 6. Instrumentation of Robot Shell

This empty shell was then placed at the top of a slightly sloped concrete slab ($\alpha \approx 2°$), inflated to a set pressure, and allowed to roll down the slope. This allowed for multiple runs with a consistent set of initial conditions since the shell alone has no actuation capabilities. Figure 7 shows screenshots of the shell undergoing the relaxation or nutation instability. As it rolls under the influence of gravity, the hubcaps roll parallel to the viewer, but as it relaxes, they roll hubcap to hubcap. Similar to the free body case illustrated in Figure 2. The scene is also included in the supplemental video.

Fig. 7. Screenshots of the shell experiencing a nutation instability, the hubcaps start parallel to the viewer, then start relaxing toward perpendicular while maintaining a steady path away

Data from an experimental run is shown on the left of Figure 8 with the relaxation angle and kinetic energy calculated in post-processing. Recall from (11) that the relaxation angle is a function of the system angular momentum, so small irregularities in the concrete and shell will affect the net system energy chaotically. A third-order Savitzky-Golay filter was employed to remove most of the noise in the angular velocity readings. The kinetic energy decreases towards the end of the tests as the robot rolls over the mounting interface from soft shell to hard hubcap which slows the system.

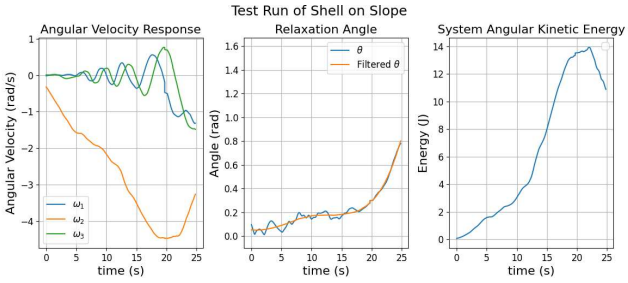

Fig. 8. Data from a single run of the shell rolling down a slope, despite increasing in energy, the system experiences the relaxation effect

For similar types of robots, the shell pressure had a significant effect on the control system [16]. Trials were conducted at two main pressure levels to determine if pressure has a significant effect on the relaxation rate. The filtered

relaxation angles were used to calculate an average relaxation rate, determining whether system pressure had a significant effect on the relaxation dynamics. In this test case, there appears to be no significant relationship between the rate of relaxation and tested pressure range, shown by the poor linear regression in Figure 9.

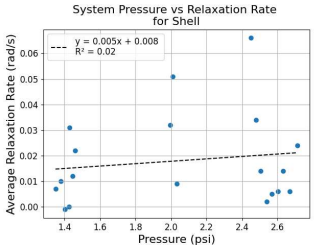

Fig. 9. Average relaxation rates at different pressures.

The lack of a noticeable effect here implies the dissipative effect of the shell ($\boldsymbol{\omega}^T C\boldsymbol{\omega}$) might not be the main driver behind the sign of $\dot{T}$ and subsequently the relaxation effect. The next section will utilize changes in rolling surfaces to loosen the kinematic constraints and subsequently $\dot{T}_{trans}$.

V. Dynamics Under Various Rolling Constraints

Adding a pendulum mechanism to the shell enables control over the shell's angular velocities. The bare shaft in the shell from Figure 6 is replaced with a reduced pendulum assembly as shown in Figure 10. This pendulum and instrumentation is identical to the one described in reference [5]. Usually, this pendulum allows for actuation in a drive axis $\hat{x}_2$, and a perpendicular steering axis. However, a 3D printed clamp was added to remove motion not about $\hat{x}_2$. This assembly was then tested on flat ground and floating in water, and the body velocities were recorded through an IMU mounted on the pendulum.

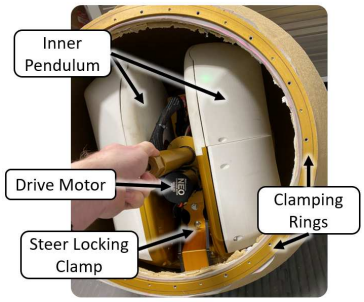

Fig. 10. Locked Steering Clamp

The stability of the relaxation dynamics for the robot rolling on flat ground now needs to include the pendulum's effects on the system. Assuming that the net moment on the body frame can be separated into $\mathbf{M} = \mathbf{M}_{pend} + \mathbf{M}_{contact}$. Where $\mathbf{M}_{contact}$ can be represented by the uniform dissipation from (3), and $\mathbf{M}_{pend}$ is the gravity torque brought on by the pendulum reflected into the shell frame, this can be compactly stated in (30) as a function of the shell's position in space ${}^{w}R_b$ and the rotated angle of the pendulum around the driveshaft, θ_d.

$$\mathbf{M}_{pend} = f({}^{w}R_b, \theta_d) \tag{30}$$

The system stability is still dependent on the sign of the new $\dot{T}$ in (31).

$$\dot{T} = \boldsymbol{\omega}^T \mathbf{M}_{pend} - \boldsymbol{\omega}^T C\boldsymbol{\omega} - \dot{T}_{trans} \tag{31}$$

This is not a trivial exercise since the pendulum forces depend on its pose with respect to gravity in the world frame and the state angles (${}^{w}R_b$ and θ_d). However, it is possible to choose M_{pend} such that the system is stable at high speeds; some examples can be found in [11, 16]. Irresponsible choices can also drive the system unstable; therefore, the sign of $\boldsymbol{\omega}^T \mathbf{M}_{pend}$ is arbitrary and can be both positive and negative. The added clamp removes actuation in the transverse direction to simplify comparison.

A series of experiments was conducted with the robot in this configuration. For each run, the robot was commanded to track a certain speed in ω_2. While rolling, an IMU attached to the pendulum assembly recorded the shell's body angular velocities. The resulting data and calculated relaxation angles are shown in Figure 11.

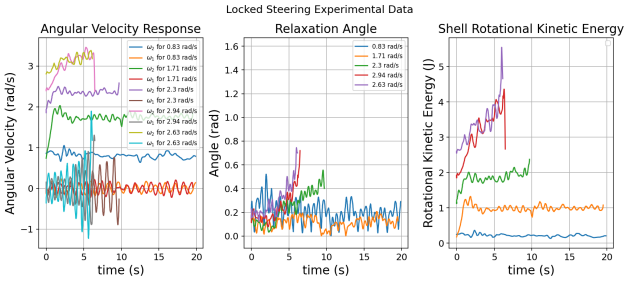

Fig. 11. Data from the robot rolling on land. As the system tracks a constant drive velocity (left). The calculated relaxation angles (center) and shell kinetic energy (right).

From the data in Figure 11, the restricted pendulum prevents the system from relaxing at slower speeds. So $\dot{T}$ is negative in this situation. However, once speeds exceed around 2 radians per second, the system's reduced pendulum no longer balances the system, and it begins to experience the relaxation effect. The system cannot maintain higher speeds without control, so those series are truncated sooner.

However, when the robot is placed in a similar situation in water, shown in Figure 12, the same pendulum could balance the system at much higher speeds. The resulting relaxation angle is shown in Figure 13.

Fig. 12. Robot rolling in water with ω_2 around 18 rad/s

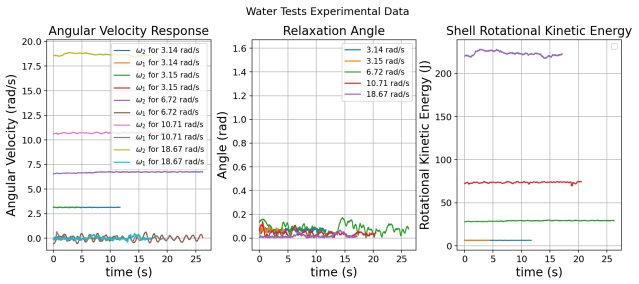

Fig. 13. Measured system velocities (left) with calculated relaxation angles (center) and shell kinetic energies (right)

Comparing the tests where the robot rolls on flat ground to those on water, the constraints given by equation (14) are no longer valid, as the robot slips significantly more on water than on land. As a result, $\dot{T}_{trans}$ as defined with that equation breaks down. So the pendulum can overcome the additional dissipation and does not experience the relaxation effect. This shows that while both $\boldsymbol{\omega}^T C \boldsymbol{\omega}$ and $\dot{T}_{trans}$ both contribute to the negative sign of $\dot{T}$, $\dot{T}_{trans}$ and the robot's constraints play a more significant role in the effect.

VI. Discussion

Switching to water to overcome the relaxation effect is rarely practical. Robot designers have two options to mitigate this effect in their prototypes: adjust the outer shells' inertial profile or adapt the control scheme.

From equations (11) and (31), a spherical system rolling about its minor moment of inertia on solid ground is inherently unstable. Redesigning the shell's inertia profile so that rolling occurs about the major moment of inertia changes the sign of the inertia ratio in the relaxation dynamics, naturally stabilizing the motion without altering the control scheme. However, the system's natural stability in water may be lost.

When redesigning is not feasible, stabilization can be achieved through control instead. The choice of $\mathbf{M}_{pend}$ in (31) is where a user-defined control law can influence the sign of $\dot{\theta}$. Deriving a suitable control law is beyond the scope of this paper, but we offer some insight on possible uses of the relaxation dynamics in a control scheme. Equation (11) has a singularity that would need to be managed when the system is at rest, i.e. $||L|| = 0$. In astrodynamics, the relaxation angle is commonly measured with a time average over its period (see ref. [3]). This is sufficient for the large timescales in the study of orbiting asteroids; however, rolling robots typically operate at much faster speeds, so this paper could not follow that reference's example. Hence the raw calculated angle is incredibly noisy in the experiments. Finding a clean representation of θ would be critical for control design. Finally, dissipation was modeled as a linear and uniform throughout the paper in Eq. (3). The actual dissipation of the system would require a more robust model and would be influenced by varied terrain softness and outer shell type. An accurate model could be used to calculate a dimensionless parameter as a predictor on the onset of the instability.

VII. Conclusion

This paper extends the theory of relaxation dynamics, well established in satellite and asteroid mechanics, to the domain of rolling spherical robots. By analyzing oblate inertial profiles under rolling constraints, we showed that the wobbling and eventual flipping observed in spherical shells are natural consequences of the relaxation effect. The derived equations, supported by experimental trials with varying internal configurations and constraint conditions, demonstrate that translational rolling constraints play a dominant role in driving this instability by acting as an additional and counterintuitive dissipation mechanism.

Looking forward, this connection between classical rotational dynamics and constrained robotic motion opens the door to new hardware and control approaches. More broadly, the relaxation framework offers a compact tool for analyzing and predicting stability in mobile rolling platforms where shape, inertia, and ground interaction are tightly coupled.

References

[1] Mark S Ashbaugh, Carmen C Chicone, and Richard H Cushman. "The twisting tennis racket". In: *Journal of Dynamics and Differential Equations* 3 (1991), pp. 67–85.

[2] Peter W Likins. *Effects of energy dissipation on the free body motions of spacecraft*. Tech. rep. Jet Propulsion Laboratory, 1966.

[3] Michael Efroimsky. "Relaxation of wobbling asteroids and comets—theoretical problems, perspectives of experimental observation". In: *Planetary and Space Science* 49.9 (2001), pp. 937–955.

[4] Aminata Diouf et al. "Spherical rolling robots—Design, modeling, and control: A systematic literature review". In: *Robotics and Autonomous Systems* 175 (2024), p. 104657.

[5] Micah Oevermann et al. "Roboball: An all-terrain spherical robot with a pressurized shell". In: *2024 IEEE International Conference on Robotics and Automation (ICRA)*. IEEE. 2024, pp. 13502–13508.

[6] Muhammad Affan Arif et al. "Design of an amphibious spherical robot driven by twin eccentric pendulums with flywheel-based inertial stabilization". In: *IEEE/ASME Transactions on Mechatronics* 28.5 (2023), pp. 2690–2702.

[7] Samira Asiri et al. "The Design and Development of a Dynamic Model of a Low-Power Consumption, Two-Pendulum Spherical Robot". In: *IEEE/ASME Transactions on Mechatronics* 24.5 (2019), pp. 2406–2415.

[8] Bruno Belzile and David St-Onge. "ARIES: Cylindrical pendulum actuated explorer sphere". In: *IEEE/ASME Transactions on Mechatronics* 27.4 (2022), pp. 2142–2150.

[9] Zhaohan Feng and Hanxu Sun. "A high-speed motion control method of pendulum driven spherical robot". In: *2021 IEEE International Conference on Artificial Intelligence and Computer Applications (ICAICA)*. IEEE. 2021, pp. 1–7.

[10] Bing Li, Qiang Deng, and Zhichao Liu. “A spherical hopping robot for exploration in complex environments”. In: *2009 IEEE International Conference on Robotics and Biomimetics (ROBIO)*. IEEE. 2009, pp. 402–407.

[11] Yixu Wang et al. “Robust servo linear quadratic regulator controller based on state compensation and velocity feedforward of the spherical robot: Theory and experimental verification”. In: *International Journal of Advanced Robotic Systems* 20.2 (2023).

[12] Tomi J Ylikorpi, Aarne J Halme, and Pekka J Forsman. “Dynamic modeling and obstacle-crossing capability of flexible pendulum-driven ball-shaped robots”. In: *Robotics and Autonomous Systems* 87 (2017), pp. 269–280.

[13] Gregory C Schroll et al. “Dynamic model of a spherical robot from first principles”. MA thesis. Colorado State University. Libraries, 2010.

[14] Animesh Singhal et al. “Pendulum actuated spherical robot: dynamic modeling & analysis for wobble & precession”. In: *IFAC-PapersOnLine* 55.22 (2022), pp. 67–72.

[15] Donghyun Kim et al. “Stabilizing Series-Elastic Point-Foot Bipeds Using Whole-Body Operational Space Control”. In: *IEEE Transactions on Robotics* 32.6 (2016), pp. 1362–1379.

[16] Derek J. Pravecek et al. “Empirically Compensated Setpoint Tracking for Spherical Robots With Pressurized Soft-Shells”. In: *IEEE Robotics and Automation Letters* 10.3 (2025), pp. 2136–2143.